Accepted Manuscript

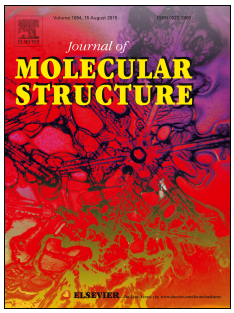

Synthesis, structure investigation and biological evaluation of 2-thiophene N(4)-phenylthiosemicarbazone and its three metal derivatives

Zilang Wang, Yuanyuan Wu, Yan Fu, Mingxue Li, Yanxue Tai, Yanke Li

PII: S0022-2860(15)30142-3

DOI: 10.1016/j.molstruc.2015.07.031

Reference: MOLSTR 21686

To appear in: *Journal of Molecular Structure*

Received Date: 20 April 2015

Revised Date: 12 July 2015

Accepted Date: 16 July 2015

Please cite this article as: Z. Wang, Y. Wu, Y. Fu, M. Li, Y. Tai, Y. Li, Synthesis, structure investigation and biological evaluation of 2-thiophene N(4)-phenylthiosemicarbazone and its three metal derivatives, *Journal of Molecular Structure* (2015), doi: 10.1016/j.molstruc.2015.07.031.

Synthesis, structure investigation and biological evaluation of 2-thiophene N(4)-phenylthiosemicarbazone and its three metal derivatives

Zilang Wang [a], Yuanyuan Wu [a], Yan Fu[a], Mingxue Li [a,*], Yanxue Tai [a], Yanke Li

[a]*Henan Key Laboratory Polyoxometalates, Institute of Molecular and Crystal Engineering, College of Chemistry and Chemical Engineering, Henan University, Kaifeng, 475004, PR China*

ABSTRACT A 2-thiophene N(4)-phenylthiosemicarbazone (**HL**) ligand and its three metal derivatives [CuL_2] (**1**), [NiL_2] (**2**) and [PdL_2] (**3**) are synthesized and characterized by elemental analysis, IR spectra, mass spectra as well as the single-crystal X-ray diffraction. Compounds **1**–**3** have the identical architectures in which the Schiff bases L^- ions act as the bibasic chelating ligands with thiolate S and imine N atoms as the donor sites. Cytotoxic studies carried out *in vitro* against human liver hepatocellular carcinoma HepG2 cells and human normal hepatocyte QSG7701 cells show that **1** can be able to inhibit cell proliferation growth. Compound **1** promotes a dose-dependent apoptosis in HepG2 cells. The potential structure-activity relationships among **HL** and **1**–**3** are further investigated by Hirshfeld surface combining fingerprint plots.

Keywords: Crystal structure; Thiosemicarbazone; Cytotoxicity; Hirshfeld surface; Structure-activity relationships

---

*Corresponding author. Tel: +86 2378 3881518, Fax: +86 2378 3881589.

E-mail address: *limingxue@henu.edu.cn* (M. -X. Li)

1. Introduction

Thiosemicarbazones and their metal complexes have received considerable attentions due to their good repeatability, various structures and beneficial pharmacological properties [1–7]. It is reported that the biological activities of thiosemicarbazones are closely related to the parent aldehyde or ketone group, amino-terminal substitution and metal ions [8-13]. Moreover, the antitumour activities of thiosemicarbazones increase with their ability coordinating to the metal ions [8–9].

Thiosemicarbazones usually coordinate to the metal ions, notable for transition metal, through the bidentate (N, S) mode or tridentate (N, N, S) mode [14–15], which are obviously affected by the types of the substituent group on the azomethine carbon. Their coordination abilities are greatly influenced by the extended delocalization of electron density over the –NH–C(S)–NH–N=C– system, which can be strengthened by the substitutions of the terminal N atom.[16] Thus, the rational design and synthesis of the specific thiosemicarbazones is still an interesting and challenging field.

In the past few decades, many transition metal complexes likely Co(II) [17], Ni(II) [18–19], Cu(II) [20], Zn(II) [21], Pd(II) [22-24], Ag(I) [25], Au(I) [26] and Pt(II) [26] related to thiosemicarbazones have been prepared and their cytotoxic activities have been investigated using different cell line cultures. However, the mechanism of action is still controversial in many respects and has not been completely identified including ribonucleotide reductase inhibition, metal dependent radical damage, DNA binding, and inhibition of protein synthesis, *etc*. Therefore, the discovery and development of new metal-based drugs remain an evergrowing area in the medicinal inorganic chemistry as usual.

In recent years, we have been working on the structural and biological properties of thiosemicarbazones and their metal complexes [17, 21, 25, 27–33]. We focus our mind on the optimization of thiosemicarbazones and the selective preference of metal ions in order to effectively enhance biological activities and reduce the potential toxicity. We have previously reported the synthesis, crystal structure and biological activities of 2-thiophene N(4)-methylthiosemicarbazone and its Ag(I) complex [25], which has taken on the better biological activities. To continue this research, herein 2-thiophene N(4)-phenylthiosemicarbazone (HL) is prepared, in which a phenyl is introduced to replace methyl with the aim of altering the

delocalization of electron density over the –NH–C(S)–NH–N=C– system and adjusting its coordination ability. Furthermore, we attempt to increase the interaction area of the non-covalent bond binding like groove binding and intercalative binding with the substrate molecule. Ultimately, their pharmacological properties can be improved and optimized. In this paper, three transition metal complexes [CuL_2] (**1**), [NiL_2] (**2**) and [PdL_2] (**3**) (Scheme 1) are successfully synthesized *via* **HL**. They are carried out *in vitro* against HepG2 cells and normal QSG7701 cells. The effect of **1** on cell apoptosis in HepG2 is studied. The possible reasons for the activity differences among **HL** and **1**-**3** are further analyzed by Hirshfeld surface combing fingerprint plots.

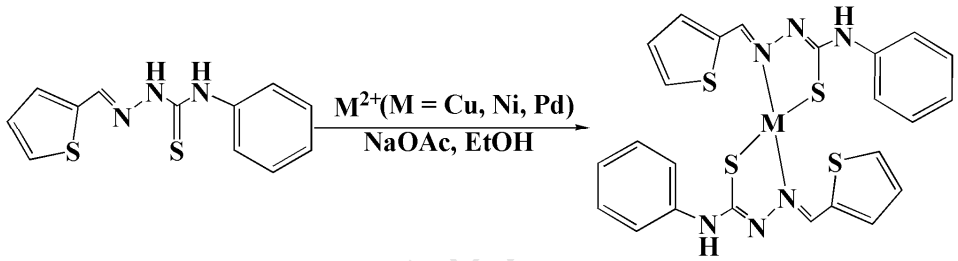

Scheme 1. The reaction scheme for the synthesis of **1**–**3**.

2. Experimental

2.1. Materials and physical measurements

All solvents and reagents were commercially available and used without further purification. Melting points were determined with a X-5 Micro Processor Melting-point Apparatus. C, H and N elemental analyses were performed on a Perkin-Elmer 240C elemental analyzer. The mass spectra (MS) were taken out on an Esquire 3000 LC-MS mass spectrometer. The infrared spectrum was recorded from KBr pellets on a Nicolet 170SXFT-IR spectrometer in the range of 400−4000 cm^{-1}.

*2.2. Synthesis of 2-thiophene N(4)-phenylthiosemicarbazone (**HL**)*

N(4)-phenylthiosemicarbazide (0.50 g, 3 mmol) is added dropwise to an ethanol solution (30 mL) of 2-thiophene (0.34 g, 3 mmol) with five drops of acetic acid as catalyst. After refluxed for 2 h, the resultant solution is filtered. Yellow powders separated on cooling are washed with ethanol and dried over P_4O_{10} in vacuo, yield 81%. Melting point: 203–204 °C. Elemental analysis calcd (%) for $C_{12}H_{11}N_3S_2$: C 55.14%, H 4.24%, N16.08%. Found: C 55.36%, H 4.47%, N 15.92%. ESI-MS. Found: *m*/*z* 284.0 [HL + Na^+]. Calcd: *m*/*z* 284.0. Colorless crystals suitable for X-ray studies are obtained by slow evaporation of its ethanol solution.

*2.3. Synthesis of [CuL_2] (**1**)*

An ethanol solution containing $Cu(ClO_4)_2 \cdot 6H_2O$ (0.074 g, 0.2 mmol) is added dropwise to an ethanol solution (20 mL) of 2-thiophene N(4)-phenylthiosemicarbazone (0.105 g, 0.4 mmol) and NaOAc (0.034 g, 0.4 mmol). After refluxing with stirring for 2 h, the resultant solution is filtered. The obtained solid product is recrystallized from ethanol and dried over P_4O_{10} in vacuo. Yield, 68%. Melting point: 199–201 °C. Elemental analysis calcd (%) for $C_{24}H_{20}CuN_6S_4$: C 49.34%, H 3.45%, N 14.38%. Found: C 49.28%, H 3.59%, N 14.20%. ESI-MS. Found: *m*/*z* 585.7 $[Cu(L)(HL)]^+$. Calcd: *m*/*z* 585.3.Violet crystals suitable for X-ray studies are obtained by slow evaporation of its ethanol solution.

*2.4. Synthesis of [NiL_2] (**2**)*

The procedure is the same as that for **1** except that $Cu(ClO_4)_2 \cdot 6H_2O$ (0.074 g, 0.2 mmol) is replaced by $Ni(ClO_4)_2 \cdot 6H_2O$ (0.073 g, 0.2 mmol). Yield, 60%. Melting point: 212–214 °C. Elemental analysis calcd (%) for $C_{24}H_{20}NiN_6S_4$: C 49.75%, H 3.48%, N 14.50%. Found: C 50.02%, H 3.56%, N 14.31%. ESI-MS. Found: *m*/*z* 578.9 $[Ni(L)(HL)]^+$. Calcd: *m*/*z* 579.0. Red crystals suitable for X-ray studies are obtained by slow evaporation of its ethanol solution.

*2.5. Synthesis of [PdL_2] (**3**)*

The procedure is the same as that for **1** except that $Cu(ClO_4)_2 \cdot 6H_2O$ (0.074 g, 0.2 mmol) is replaced by $PdCl_2$ (0.035 g, 0.2 mmol). Yield, 55%. Melting point: 198–200 °C. Elemental analysis calcd (%) for $C_{24}H_{20}PdN_6S_4$: C 45.96%, H 3.21%, N 13.40%. Found: C 45.28%, H 3.39%, N 13.20%. ESI-MS. Found: *m*/*z* 629.3 $[Ni(L)(HL)]^+$. Calcd: *m*/*z* 628.1. Orange crystals suitable for X-ray studies are obtained by slow evaporation of its ethanol solution.

2.6. X-ray crystallography

Single crystal X-ray data collection are performed on a Bruker SMART APEX CCD area-detector diffractometer equipped with a graphite-monochromated Mo$K\alpha$ radiation (λ = 0.71073 Å) at 293 (2) K. The intensities are corrected for Lorentz and polarization effects and for empirical absorption. The structure is solved by direct methods and refined by full-matrix least-squares techniques based on F^2 using SHELXS–97 and SHELXL–97 programs [34], respectively. All non-hydrogen atoms are refined anisotropically. All remaining H atoms were positioned geometrically. A summary of the crystal data and refinement results are listed in Table 1. Selected bond lengths are given in Table 2.

Table 1 Summary of crystal data and refinement results for **HL** and **1–3.**

	HL	**1**	**2**	**3**
Empirical formula	$C_{12}H_{11}N_3S_2$	$C_{24}H_{20}CuN_6S_4$	$C_{24}H_{20}NiN_6S_4$	$C_{24}H_{20}PdN_6S_4$
Formula weight	261.36	584.29	579.41	627.10
Crystal size /mm	0.58×0.40×0.07	0.46×0.34×0.07	0.56×0.49×0.11	0.48×0.37×0.08
Crystal system	Triclinic	Monoclinic	Orthorhombic	Orthorhombic
Space group	*P*–1	*P*2(1)/*c*	*Pbca*	*Pbca*
T /K	296(2)	296(2)	296(2)	296(2)
a /Å	5.724(11)	7.105(4)	9.8627(15)	10.0707(10)
b /Å	10.09(19)	7.507(4)	7.8100(12)	7.7048(7)
c /Å	11.56(2)	24.771(14)	32.299(5)	32.526(3)
V Å ^{3}	629.6(2)	1291.7(12)	2487.9(7)	2523.7(4)
α (°)	72.374(3)	90.00	90.000	90.00
β (°)	81.929(4)	102.143(18)	90.000	90.00
γ (°)	88.249(4)	90.00	90.000	90.00
D_c /g cm^{-3}	1.379	1.502	1.547	1.650
Z	2	2	4	4
μ /mm^{-1}	0.403	1.194	1.142	1.093
θ (°)	1.87–26.00	2.84–25.00	2.42–25.00	2.38–25.00
F_{000}	272	598	1192	1264
Index ranges	$-6 \le h \le 7$,	$-8 \le h \le 8$,	$-11 \le h \le 11$,	$-11 \le h \le 11$,
	$-12 \le k \le 9$,	$-8 \le h \le 8$,	$-9 \le k \le 9$,	$-7 \le h \le 9$,
	$-14 \le l \le 13$	$-18 \le l \le 29$,	$-17 \le l \le 38$	$-38 \le l \le 34$,
Refl. collected	3472	6206	10379	11795
Refl. unique	2432	2248	2168	2212
R_{int}	0.0538	0.0894	0.1230	0.0767
Parameters	154	160	161	160
R_1,wR_2 [$I \ge 2\sigma$ (I)]	0.0595, 0.1602	0.0807, 0.1845	0.0509, 0.1095	0.0309, 0.0491
R_1,wR_2 (all date)	0.0919, 0.1739	0.1198, 0.1949	0.0979, 0.1335	0.0644, 0.0538
Goodness-of-fit on F^2	0.856	0.873	0.744	0.756

Table 2 Selected bond lengths (Å) and bond angles (°) for **HL** and **1**–**3** [a].

HL		**1**		**2**		**3**	
S(1)-C(7)	1.673(4)	Cu(1)-N(3)#1	1.978(7)	Ni(1)-N(3)	1.882(4)	Pd(1)-N(3)#1	2.011(3)
N(1)-C(7)	1.336(5)	Cu(1)-N(3)	1.978(7)	Ni(1)-N(3)#1	1.882(4)	Pd(1)-N(3)	2.011(3)
N(1)-C(6)	1.433(5)	Cu(1)-S(1)	2.265(3)	Ni(1)-S(1)#1	2.1679(15)	Pd(1)-S(1)#1	2.2929(10)
N(2)-C(7)	1.341(5)	Cu(1)-S(1)#1	2.265(3)	Ni(1)-S(1)	2.1679(15)	Pd(1)-S(1)	2.2929(10)
N(2)-N(3)	1.378(4)	S(1)-C(7)	1.741(9)	S(1)-C(7)	1.727(5)	S(1)-C(7)	1.747(3)
N(3)-C(8)	1.288(5)	N(1)-C(7)	1.359(10)	N(1)-C(7)	1.361(6)	N(1)-C(7)	1.366(4)
C(1)-C(6)	1.373(5)	N(1)-C(6)	1.424(11)	N(1)-C(6)	1.413(6)	N(1)-C(6)	1.403(4)
C(1)-C(2)	1.376(6)	N(2)-C(7)	1.308(10)	N(2)-C(7)	1.301(6)	N(2)-C(7)	1.299(4)
C(2)-C(3)	1.360(6)	N(2)-N(3)	1.388(8)	N(2)-N(3)	1.403(5)	N(2)-N(3)	1.394(3)
C(3)-C(4)	1.382(6)	N(3)-C(8)	1.311(9)	N(3)-C(8)	1.299(6)	N(3)-C(8)	1.296(4)
C(12)-S(2)-C(9)	92.6(2)	N(3)#1-Cu(1)-N(3)	180.0(3)	N(3)-Ni(1)-N(3)#1	180.0(1)	N(3)#1-Pd(1)-N(3)	180.00(11)
C(7)-N(1)-C(6)	127.6(3)	N(3)#1-Cu(1)-S(1)	96.9(2)	N(3)-Ni(1)-S(1)#1	94.74(14)	N(3)#1-Pd(1)-S(1)#1	82.59(9)
C(7)-N(2)-N(3)	120.6(3)	N(3)-Cu(1)-S(1)	83.1(2)	N(3)#1-Ni(1)-S(1)#1	85.26(14)	N(3)-Pd(1)-S(1)#1	97.41(9)
C(8)-N(3)-N(2)	116.9(3)	N(3)#1-Cu(1)-S(1)#1	83.1(2)	N(3)-Ni(1)-S(1)	85.26(14)	N(3)#1-Pd(1)-S(1)	97.41(9)
C(1)-C(6)-N(1)	121.1(4)	N(3)-Cu(1)-S(1)#1	96.9(2)	N(3)#1-Ni(1)-S(1)	94.74(14)	N(3)-Pd(1)-S(1)	82.59(9)
C(5)-C(6)-N(1)	118.4(3)	S(1)-Cu(1)-S(1)#1	180.00(6)	S(1)#1-Ni(1)-S(1)	180.0	S(1)#1-Pd(1)-S(1)	180.0

[a] Symmetry transformations used to generate equivalent atoms: $-x+1, -y+1, -z$; $-x+2, -y, -z+1$; $-x+1, -y, -z+1$ for **1**–**3**, respectively.

2.7. Cytotoxicity assay [27]

The 3-(4, 5-dimethylthiazol-2-yl)-2, 5-diphenyltetrazolium bromide (MTT) assay is carried out to evaluate cytotoxicity. Cells are plated into 96-well plates at a cell density of 1×10^4 cells per well and allowed to grow in a CO_2 incubator. After 24 h, the medium is removed and replaced by fresh medium containing the tested compounds which are dissolved in DMSO at 0.01 M and diluted to various concentrations with phosphate-buffered saline (PBS) before the experiment, and the final concentration of DMSO is lower than 1%. After 24 h of incubation, cultures are incubated in 100 μL of medium with 10 μL of 5 mg mL^{-1} MTT solution for 4 h at 37 °C. The medium with MTT is removed, and 100 μL of DMSO was added to each well to dissolve the formazan. The absorbance at 570 nm is measured using a microplate reader (Bio-Tek ELX800, USA). The inhibitory percentage of each compound at various concentrations is calculated, and the IC_{50} value is determined.

2.8. Apoptosis analysis [27]

To examine whether the cytotoxicity of **1** is due to apoptosis, cell apoptosis is determined by morphologic observation and Annexin V-FITC. For morphologic observation, cells are stained with acridine orange (AO) and ethidium bromide (EB) and assessed by fluorescence microscopy. Briefly, 1 μL of a stock solution (100 μg mL^{-1} AO and EB) was added to 25 μL of a cell suspension. EB-negative cells with nuclear shrinkage, blebbing, and apoptotic bodies are counted as apoptotic cells.

3. Result and discussions

*3.1. Structural features of **HL** and **1–3***

Molecular structures of the title compounds **HL** and **1**–**3** are shown in Fig. 1. For **HL**, thiolate S(1) atom is trans to imine N(3) atom so that **HL** is not propitious to combine a metal ion as chelating ligand. Relevant N(3)–C(8) 1.288(5) Å, N(2)–N(3) 1.378(4) Å and C(7)–S(1) 1.673(4) Å bond lengths show that –N(2)H–N(3)=C(8)– and –C(7)=S(1) modes exist in **HL** as observed in other free unsubstituted thiosemicarbazides [14, 35]. **HL** at (*x*, *y*, *z*) and the other molecule at (–*x*, –*y*+1, –*z*+1) are linked together through a pair of N(2)–H···S(1) hydrogen bonds building a $R^2_2(6)$ ring, which helps to stabilize the structure packing.

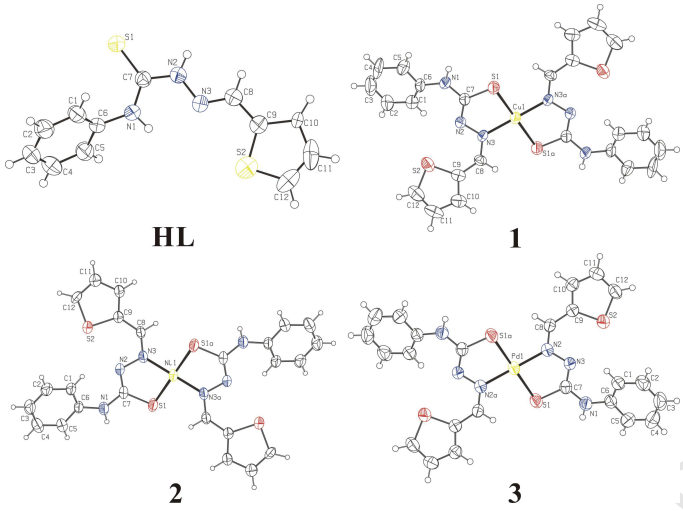

Fig.1. Molecular structures of compounds **HL** and **1**–**3**, showing the atom numbering scheme. Displacement ellipsoids are drawn at the 30% probability level. H atoms not involved in hydrogen bonding have been omitted for clarity. Symmetry codes (*a*): $-x+1, -y+1, -z$ in **1**; $-x+2, -y, -z+1$in **2**; $-x+1, -y, -z+1$ in **3**.

Through **HL,** three compounds **1-3** having the identical structures are successfully synthesized. H atom bound to N(2) finally separate resulting in a L^- anion in **1-3**. Compound **1** has an inversion center at Cu^{2+} site, which is coordinated by two L^- anions through two N(3) atoms [Cu(1)–N(3) 1.978(7) Å] and two S(1) atoms [Cu(1)–S(1) 2.265(3) Å] forming a regular parallelogram. After L^- ion coordinating to Cu^{2+} ion, the related C(7)=S(1) and C(7)–N(2) bond modes in **HL** are obviously changed to C(7)–S(1) and C(7)=N(2) bond modes in **1,** which can be proved by the obvious changes of the corresponding bond lengths. For **2,** bond distances round Ni^{2+} ion are Ni(1)–N(3) 1.882(4) Å and Ni(1)–S(1) 2.1678(15) Å, respectively. The corresponding C(7)–S(1) and C(7)–N(2) bond lengths are 1.728(5) and 1.299(6) Å. For **3,** Pd(1)–N(3) and Pd(1)–S(1) bond lengths are 2.011(3) and 2.2929(10) Å, respectively. Additionally, the related C(7)–S(1) and C(7)–N(2) bond distances are 1.747(3) and 1.299(4) Å. These results fully indicate the related C(7)=S(1) and C(7)–N(2) bond modes in **HL** are also changed to C(7)–S(1) and C(7)=N(2) bond modes in **2**–**3**.

3.2. Infrared spectra study

The characteristic vibrational bands of **HL** and **1**–**3** corresponding to the important functions in the system are presented in Table 3. The free ligand **HL** shows two bands at 3300 and 3141 cm^{-1} assigned to N–H stretching vibrations, which are observed at 3379, 3381 and 3381 cm^{-1} in

complexes **1**–**3** [27], respectively. A strong absorption at 1546 cm^{-1} is attributed to ν(C=N) in **HL**. The decrease in frequency of ν(C=N) band for three compounds compared to that in **HL** indicating that the coordination is through imine N atom. The obviously increase in frequency of ν(N–N) band from 1204 cm^{-1} in **HL** to 1245, 1250, 1247 cm^{-1} in **1**–**3** further support the coordination of imine N atom. A band appeared at 854 cm^{-1} is assigned to ν(C=S) in **HL,** which has been shifted to lower frequency 823, 830 and 830 cm^{-1} in **1**–**3** suggesting that the coordination of thiolate S atom through –C–S–Metal mode after enolization followed by deprotonation on sulfur [3, 14].

Table 3 IR spectral assignment for **HL** and **1–3** (cm^{-1}).

Compounds	ν (N–H)	ν(C=N)	ν(N–N)	ν(C=S)
HL	3300, 3141	1546	1204	854
1	3379	1525	1245	823
2	3381	1502	1250	830
3	3381	1496	1247	830

3.3. Cytotoxicity assay

The ability of $Cu(ClO_4)_2{\cdot}6H_2O$, **HL** and three metal compounds to inhibit growth of HepG2 and QSG7701 cells are tested. Herein Mitoxantrone is used as the reference compound for comparison. Comparison of the cytotoxic activities indicates **1** has much lower IC_{50} value (12.71 ± 1.22, 13.12 ± 0.53 μM) with the better cytotoxicity (Fig. 2). $Cu(ClO_4)_2{\cdot}6H_2O$, **HL** and **2**–**3** have no antitumor activity at all. For **1**, it is necessary to make embedded study in the mechanism of action

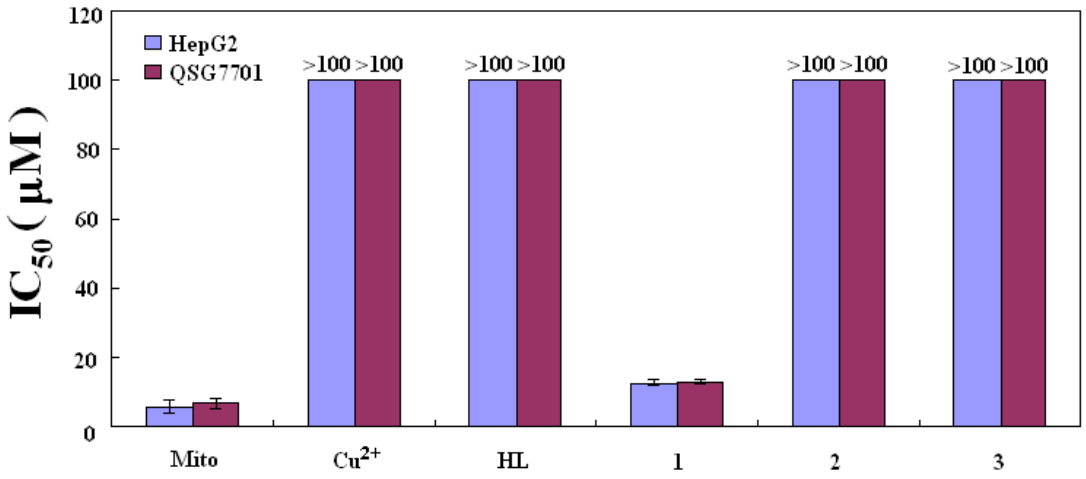

Fig. 2. The cytotoxicity of $Cu(ClO_4)_2$, **HL** and **1-3** on tumor cells and normal cells. Mitoxantrone

(Mito) is used as reference.

3.3.1 Effect of 1 on cell apoptosis

Green live cells with normal morphology are observed in control group (Fig. 3). Green early apoptotic cells with nuclear margination and chromatin condensation and orange later apoptotic cells with fragmented chromatin and apoptotic bodies are observed after **1** treatment. The results suggest that **1** can induce liver cancer cells apoptosis *in vitro.*

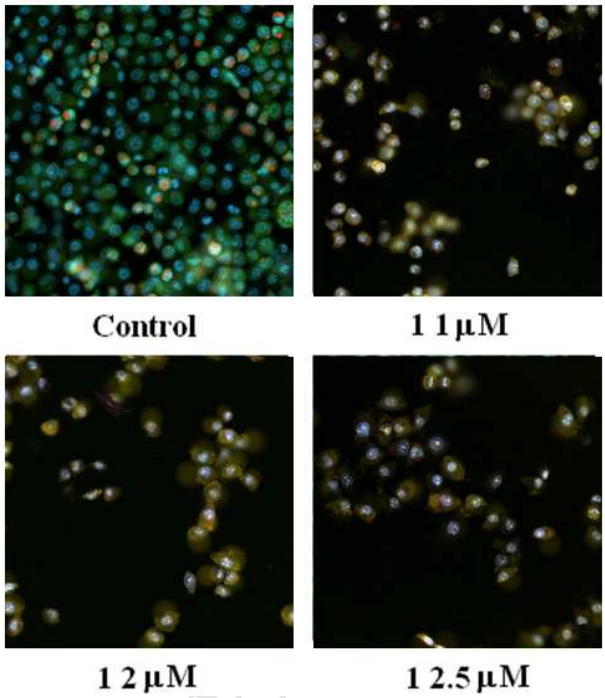

Fig. 3. Morphologic observation of HepG2 cell apoptosis is determined by AO/EB staining with the indicated concentrations of **1** for 48 h.

3.4. Hirshfeld surface analysis

Hirshfeld surfaces combining fingerprint plots generated by the Crystalexplorer **2.1** software [36] can identify the types and regions of intermolecular interactions and the proportion of this interaction to the total Hirshfeld surfaces area. Molecular Hirshfeld surfaces in crystal structure are constructed from the electron distribution. The normalized contact distances (d_{norm}) based on both d_e, d_i and the *vdw* radii of the atom are listed in the following equation. The 2D fingerprint plot is the combination of d_e and d_i [37–39].

$$d_{norm} = (d_i - r_i^{vdw})/ r_i^{vdw} + (d_e - r_e^{vdw})/r_e^{vdw}$$

Hirshfeld surfaces for **HL** and **1**–**3** have been mapped over d_{norm}, shape index and curvedness (Fig. 4*a*-*c*), respectively. As shown in Fig. 4*a*, deep red areas are corresponding to the metal–N and

metal–S bonds. The interactions between thiolate S atom and H atoms bound to N are shown as pale red areas in the Hirshfeld surfaces. Visible spots are attributed to the H···H contacts. The intermolecular N–H···Sinteractions with 23.6%, 20.5%, 17.2% and 16.3% contribution to the total Hirshfeld surface for **HL** and **1**–**3** appear as two distinct spikes in the 2D fingerprint plots (Fig. 5*a*-*b*). The lower spike attributes to S atoms interacting with H atoms bound to the nitrogen atoms, the upper spike being N–H atoms interacting with S atoms. C···H/H···C contacts constitute 24.2%, 24.7%, 27.6% and 26.7% (Fig. 5*a*, *c*) of the total Hirshfeld surface attributing to the C–H··π interactions for HL and **1**–**3**, which can also be seen from the pairs of typical 'wings' appear at the top left and bottom right of the two-dimensional fingerprint plots. The scattered points spread up to $d_i = d_e \approx 1.0$ Å are corresponding to the H···H interactions (contribution comprising: 38.1%, 33.0%, 32.1% and 32.7% for **HL** and **1**–**3**) in the fingerprint plots (Fig. 5*a*). In these compounds, π-π interactions are not observed because the adjacent red and blue triangles are not present in the shape index surface. Additionally, π-π interactions are not evident on the curvedness as a large flat region across the molecule [39]. After **HL** ligands are converted into metal coordination complexes **1**-**3**, the proportion of N–H···S and H···H interaction comprising slightly decrease and C–H··π interaction constituting increase slightly, which suggest metal-chelating has little influence on the shape and flexibility of **HL** ligand.

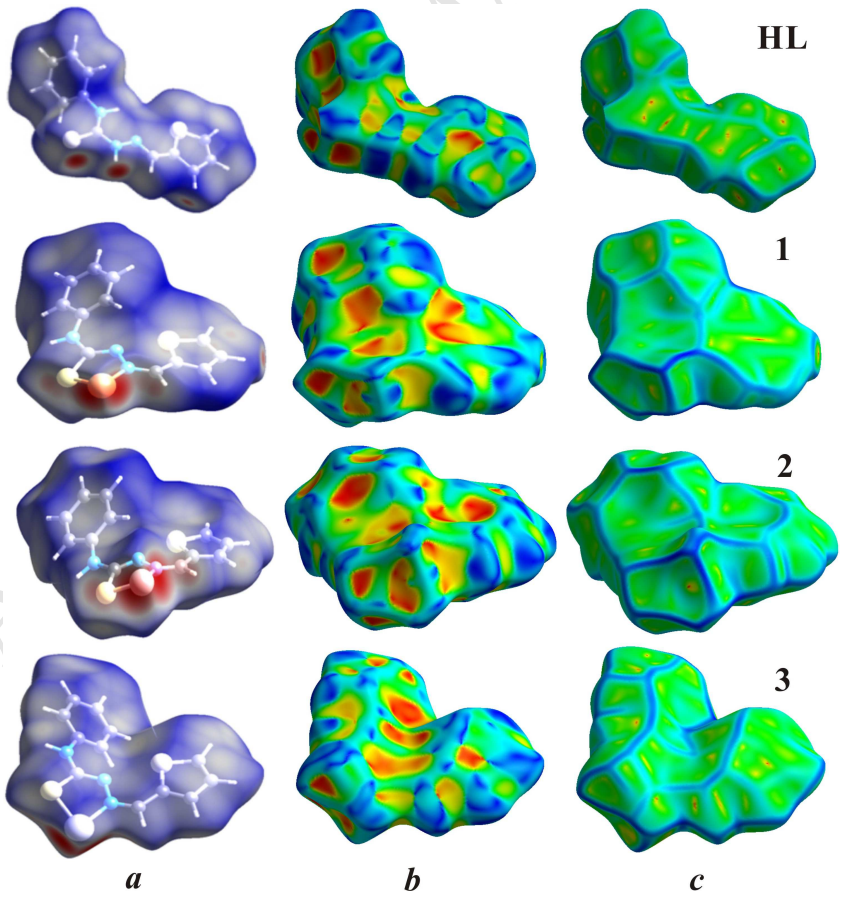

Fig. 4. Hirshfeld surface: (*a*) d_{norm}, (*b*) shape index and (*c*) curvedness for **HL** and **1**–**3**.

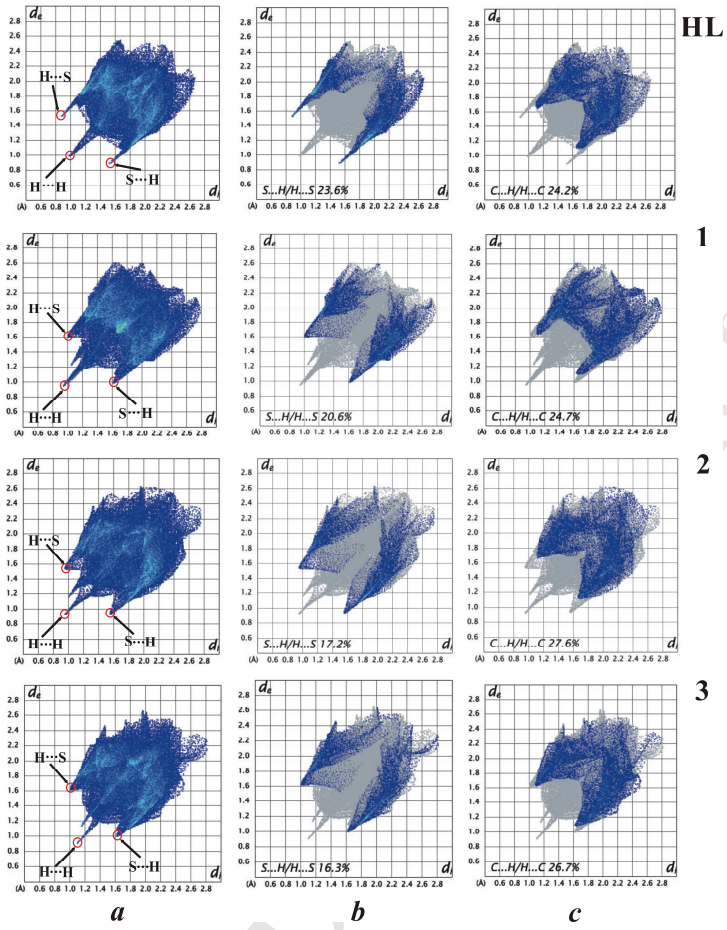

Fig. 5. Fingerprint plots of **HL** and **1–3**: (*a*) full and involving (*b*) S···H/S···H and (*c*) C···H/H···C contacts showing the proportion of contacts contributing to the total Hirshfeld surface area of molecules**.**

3.5. Structure–activity relationships

Under the same experiment condition, $Cu(ClO_4)_2{\cdot}6H_2O$ and **HL** have no cytotoxicity at all. For **1–3,** although they have the identical structures, only **1** embodies the better biological activities. On the one hand, coordination plays an important role in cytotoxic dose reduction. On the other hand, the types of metal ion play key roles in the growth inhibitory activity [40]. Therefore, the perfect matching between **HL** and transition metal results in their finally biological activity.

The investigation results of Hirshfeld surface analysis combining fingerprint plots and cytotoxic studies signify that the action between **1** and the substrate molecule is not the non-covalent bond binding like electrostatic binding, groove binding and intercalative binding, *et al*. We deduce the mode may be covalent bond binding or other way. Tetrahedral Cu^{2+} having the poorer stability in

the solution can be easily interacted by other donor atoms and changed into square pyramid or octahedron resulting in the biological activity. In the future, it is necessary to make further biological evaluation *in vivo*.

4. Conclusions

In summary, 2-thiophene N(4)-phenylthiosemicarbazone (**HL**) ligand and its three relevant metal derivatives [CuL_2] (**1**), [NiL_2] (**2**) and [PdL_2] (**3**) have been successfully synthesized and characterized. Cytotoxic studies are carried *in vitro* against HepG2 cells and normal QSG7701 cells, which illustrates that original ligand **HL** has no biological activity. For its three coordination compounds having identical structures, only **1** is able to inhibit cell proliferation growth. The results indicate the better matching between **HL** and metal ion determines their final biological activity. The apoptotic mechanism for **1** is evaluated in HepG2 cells. The structure-activity relationships for **HL** and **1–3** have been deeply investigated by Hirshfeld surface combing fingerprint plots, which shows that the action mode between **1** and the substrate molecule is not the non-covalent bond binding. In this paper, inactive **HL** has been successfully transformed into an active coordination compound. Unfortunately, **1** cannot well distinguish HepG2 cells from QSG7701 cells. So, this problem will need to be further gone into.

Appendix A.Supplementarymaterial

CCDC numbers 1023272–1023275 for complexes **HL** and **1–3**, respectively. These crystallographic data for this paper can be obtained free of charge via www.ccdc.cam.ac.uk/conts/ retrieving.html.

Acknowledgements

This work was financially supported by the National Natural Science Foundation of China (21071043) and the Natural Science Foundation of Henan Province (132300410146) and the Natural Science Foundation of the Educational Department of Henan Province (14B150028).

References

[1] T. S. Lobana, R. Sharma, G. Bawa, S. Khanna, Coord. Chem. Rev. 253 (2009) 977–1055.

[2] S. B. Novakovic, G. A. Bogdanovic, V. M. Leovac, Polyhedron. 25 (2006) 1096–1104.

[3] K. Alomar, A. Landreau, M. Kempf, M. A. Khan, M. Allain, G. Bouet, J. Inorg. Biochem., 104 (2010) 397–404.

[4] K. J. Duffy, A. N. Shaw, E. Delorme, S. B. Dillon, C. Erickson-Miller, L. Giampa, Y. Huang, R.

M. Keenan, P. Lamb, N. Liu, S.G. Miller, A. T. Price, J. Rosen, H. Smith, K. J. Wiggall, L. Zhang, J. I. Luengo, J. Med. Chem. 45 (2002) 3573–3575.

[5] H. Beraldo and D. Gambinob, Mini-Rev. Med. Chem. 4 (2004) 31–39.

[6] X. Du, C. Guo, E. Hansel, P. S. Doyle, C. R. Caffrey, T. P. Holler, J. H. McKerrow, F. E. Cohen, *J. Med. Chem*., 2002, 45, 2695–2707.

[7] G. Pelosi, F. Bisceglie, F. Bignami, P. Ronzi, P. Schiavone, M. C. Re, C. Casoli, E. Pilotti, J. Med. Chem. 53 (2010) 8765–8769.

[8] T. Ismail, D. Rossouw, P. Beukes, J. P. Slabbert, G. S. Smith, Inorg. Chem. Commun. 33 (2013) 154–157.

[9] P. Chellan, T. Stringer, A. Shokar, P. J. Dornbush, G. Vazquez-Anaya, K. M. Land, K. Chibale, G. S. Smith, J. Inorg. Biochem. 105 (2011) 1562–1568.

[10] M. E. Hossain, M. N. Alam, J. Begum, M. A. Ali, M. Nazimudhin, F. E. Smith, R. C. Hynes, Inorg. Chim. Acta. 249 (1996) 207–213.

[11] U. Abram, K. Ortner, R. Gust, K. Sommer, J. Chem. Soc., Dalton. Trans. (2000) 735–744.

[12] A. P. Rebolledo, M. Vieites, D. Gambino, O. E. Piro, E. E. Castellano, C. L. Zani, E. M. Souza-Fagundes, L. R. Teixeira, A. A. Batista, H. Beraldo, J. Inorg. Biochem. 99 (2005) 698–706.

[13] H. N. Hung, J. J. Jegathesh, P. I. D. Maia, V. M. Deflon, R. Gust, S. Bergemann, U. Abram, Inorg. Chem. 48 (2009) 9356–9364.

[14] K. Sampath, S. Sathiyaraj, C. Jayabalakrishnan, Spectrochimica Acta Part A. 115(2013) 287–296.

[15] A. A. Ali, H. Nimir, C. Aktas, V. Huch, U. Rauch, K. H. Schäfer, M. Veith, Organometallics. 31 (2012) 2256–2262.

[16] P. Kalaivani, R. Prabhakaran, M. V. Kaveri, R. Huang, R. J. Staples, K. Natarajan, Inorg. Chim. Acta., 2013, 405, 415–426.

[17] X. F. Zhu, Y. H. Fan, Q. Wang, C. L. Chen, M. X. Li, J. W. Zhao, J. Zhou, Russ. J. Coord. Chem. 38 (2012) 478–483.

[18] E. Pahontu, V. Fala, A. Gulea, D. Poirier, V. Tapcov, T. Rosu, Molecules. 18 (2013) 8812–8836.

[19] T. S. Lobana, P. Kumari, A. Castineiras, R. J. Butcher, Eur. J. Inorg. Chem. (2013) 3557–3566.

[20] M. Shebl, M. A. Ibrahim, S. M. E. Khalil, S. L. Stefan, H. Habib, Spectrochim. Acta, Part A.115(2013) 399–408.

[21] M. X. Li, L. Z. Zhang, C. L. Chen, J. Y. Niu, B. S. Ji, J. Inorg. Biochem. 106 (2012) 117–125.

[22] J. M. Antelo, L. Adrio, B. Bermúdez, J. Martínez, M. T. Pereira, J. M. Ortigueira, M. López-Torres, J. M. Vila, J. Organomet. Chem. 740 (2013) 83–91.

[23] M. Adams, C. Kock, P. J. Smith, K. Chibale, G. S. Smith, J. Organomet. Chem. 736 (2013) 19–26.

[24] A. I. Matesanz, C. Hernández and P. Souza, J. Organomet. Chem. 751(2014) 374–378.

[25] M. X. Li, D. Zhang, L. Z. Zhang , J. Y. Niu, Inorg. Chem. Commun. 13 (2010) 1268–1271.

[26] K. S. O. Ferraz, J. G. Da Silva, F. M. Costa, B. M. Mendes, B. L. Rodrigues, R. G. Santos, H. Beraldo, Biometals. 26 (2013) 677–691.

[27] N. Zhang, Y. X. Tai, M. X. Li, P. T. Ma, J. W. Zhao, J. Y. Niu, Dalton Trans. 43 (2014) 5182–5189.

[28] M. X. Li, M. Yang, J. Y. Niu, L. Z. Zhang, S. Q. Xie, Inorg. Chem. 51 (2012) 12521–12526.

[29] M. X. Li, Y. L. Lu, M. Yang, Y. K. Li, L. Z. Zhang, S. Q. Xie, Dalton Trans. 41 (2012) 12882–12887.

[30] M. X. Li, L. Z. Zhang, M. Yang, J. Y. Niu, J. Zhou, Bioorg. Med. Chem. Lett. 22 (2012) 2418–2423.

[31] L. Z. Zhang, G. Y. An, M. Yang, M. X. Li, X. F. Zhu, Inorg. Chem. Commun. 20 (2012) 37–40.

[32] Y. K. Li, M. X. Li, H. Yu, H. C. Wu, S. Q. Xie, Bioorg. Med. Chem. Lett. 23 (2013) 2288–2292.

[33] M. Yang, Y. L. Lu, M. X. Li, X. W. Xu, L. Chen, Inorg. Chem.Commun. 35(2013) 117–121.

[34] G. M. Sheldrick, SHELXS/L-97, University of Göttingen, Göttingen (Germany) 1997.

[35] A. Sethukumar, C. U. Kumar, R. Agilandeshwari and B. A. Prakasam, J. Mole. Struct. 1047 (2013) 237–248.

[36] S. K. Wolff, D. J. Grimwood, J. J. McKinnon, D. Jayatilaka, M. A. Spackman, *CrystalExplorer 2.1,* University of Western Australia, Perth, Australia 2007.

[37] S. K. Seth, G. C. Maity, T. Kar, J. Mol. Struct. 1000 (2011) 120–126.

[38] M. A. Spackman, J. J. McKinnon, CrystEngComm. 4 (2002) 378–392.

[39] S. K. Seth, I. Saha, C. Estarellas, A. Frontera, T. Kar, S. Mukhopadhyay, Cryst. Growth Des., 11 (2011) 3250–3265.

[40] T. Murafuji, Y. Miyoshi, M. Ishibashi, A. F. M. Rahman, Y. Sugihara, I. Miyakawa, H. Uno, J. Inorg. Biochem. 98 (2004) 547–552.

>Heterocyclic thiosemicarbazone>Cytotoxic studies>Hirshfeld surface >Fingerprint plots